PAPER

Progress of the CFETR design

To cite this article: G. Zhuang *et al* 2019 *Nucl. Fusion* **59** 112010

IOP Publishing | International Atomic Energy Agency Nuclear Fusion

Nucl. Fusion **59** (2019) 112010 (14pp) https://doi.org/10.1088/1741-4326/ab0e27

Progress of the CFETR design

G. Zhuang[1], G.Q. Li[2], J. Li[2], Y.X. Wan[1,2], Y. Liu[3], X.L. Wang[4], Y.T. Song[2], V. Chan[1,5], Q.W. Yang[3], B.N. Wan[2], X.R. Duan[3], P. Fu[2], B.J. Xiao[2] and the CFETR Design Team[1,2,3,4]

[1] University of Science and Technology of China, Hefei 230026, People's Republic of China
[2] Institutes of Plasma Physics, CAS, Hefei 230031, People's Republic of China
[3] Southwest Institute of Physics, Chengdu 610041, People's Republic of China
[4] China Academy of Engineering Physics, Mianyangc 621900, People's Republic of China
[5] General Atomic, San Diego, CA, United States of America

E-mail: gezhuang@ustc.edu.cn

Received 22 November 2018, revised 23 February 2019
Accepted for publication 8 March 2019
Published 5 June 2019

Abstract

The Chinese Fusion Engineering Testing Reactor (CFETR), complementing the ITER facility, is aiming to demonstrate fusion energy production up to 200 MW initially and to eventually reach DEMO relevant power level 1 GW, to manifest a high duty factor of 0.3–0.5, and to pursue tritium self-sufficiency with tritium breeding ratio (TBR) >1. The key challenge to meet the missions of the CFETR is to run the machine in steady state (or long pulse) and high duty factor. By using a multi-dimensional code suite with physics-based models, self-consistent steady-state and hybrid mode scenarios for CFETR have been developed under a high magnetic field up to 6.5 T. The negative-ion neutral beam injection together with high frequency electron cyclotron wave and lower hybrid wave (and/or fast wave) are proposed to be used to drive the current. Subsequently the engineering design of CFETR including the magnet system, vacuum system, tritium breeding blanket, divertor, remote handling and maintenance system will be introduced. Some research and development (R&D) activities are also introduced in this paper.

Keywords: CFETR, tritium self-sufficiency, steady-state operation, fusion reactor design

(Some figures may appear in colour only in the online journal)

1. Introduction

Nuclear fusion is one of the most promising options that can provide a large amount of clear energy with a relatively small impact on the environment. After several decades of research and development (R&D) on the magnetic confinement fusion, many of the scientific and technical hurdles in fusion have now been overcome. At present, the most critical challenge in magnetic confined fusion is to prove fusion can work on a power plant scale. Therefore, the ITER project is a necessary step on the road to generate fusion energy up to a power plant scale. The overall objective of the ITER project is to exploit the scientific and technological feasibility of magnetic confinement fusion energy. However, the ITER is still an experimental reactor and not for commercial purposes. Therefore, a fusion demonstration power plant (DEMO) is another necessary step for achieving the production of fusion energy for peaceful use.

As presented in the last IAEA Fusion Energy Conference [1], the Chinese fusion community has put forward the Chinese Fusion Engineering Testing Reactor (CFETR) project, which is targeted to build up the science and technology base for the prototype of a fusion power plant (PFPP). The roadmap of Chinese magnetic fusion energy development and the role of the CFETR has been shown and discussed in [1]. The CFETR is proposed to bridge the gap between the ITER and the first commercial fusion power plant, a necessary complement of the ITER. The primary missions of the CFETR project are proposed to demonstrate the fusion energy production of 200–1000 MW, generate the steady-state burning plasmas with duty time of about 50% and test the self-sustainable burning state with fusion gain, Q, about 20–30, in which the alpha particle heating resulted from the fusion reactions dominates all other forms of plasma heating with a fraction around 80%. Besides, realizing the tritium self-breeding with the tritium

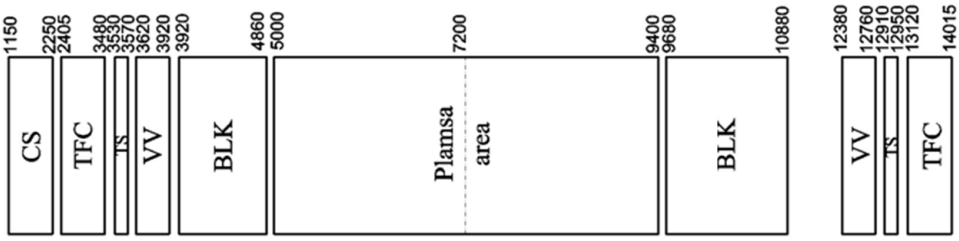

Figure 1. Radial build-up of components at mid-plane. The components include a CS (central solenoid), TFC (toroidal field coil), TS (thermal shield), VV (vacuum vessel), BLK (blanket) and plasma.

breeding ratio (TBR) of $\geqslant$1.0 and carrying out the R&D for the structural and functional materials, which should have a high neutron flux resistive, are the missions to be proposed.

The CFETR concept design has been carried out for nearly eight years (2010–2017) and can be divided into two periods. For the first period (2010–2015), in order to reduce the construction costs, the concept design is based on a small-size machine with major/minor radius $R = 5.7$ m/$a = 1.6$ m and $B_T = 4$–5 T. The second period starts from 2015, the concept design diverts from the small-size machine to a larger one with $R = 6.6$ m/$a = 1.8$ m, $B_T = 6$–7 T, aiming to achieve a target to produce over 1 GW of fusion power with attainable technical solutions. Since 2017, physics design was mainly concerned with operating scenarios, and a couple of key engineering designs, along with the R&D activities including full-size vacuum vessel (VV) manufacture, tritium breeding technology development, first wall (FW) and divertor materials, have been carried out. After careful consideration of the results from the previous CFETR concept design and the R&D activities, and as well to fulfil the goals and missions of the CFETR, a new design version of the CFETR key parameters is put forward for governing the physics and engineering designs. The present parameters of the CFETR are major radius $R = 7.2$ m, minor radius $a = 2.2$ m, a specified plasma shape with the elongation κ of 2, the toroidal magnetic field B_T at major radius of 6.5 T, the plasma current I_p of 14 MA, and the divertor configuration suggested to be lower single null configuration. Figure 1 shows the radial build-up of components at mid-plane.

The CFETR research plan will take a two-stage approach, as shown in the roadmap in [1]. The first stage is to establish the steady-state DT plasmas producing fusion power of no less than 200 MW, $Q = 1$–5, and TBR > 1.0 and a neutron dose requirement of ~10 dpa (displacements per atom). The second stage is to do the DEMO validation and produce net electric power with fusion power of >1 GW, $Q > 10$, and a neutron dose requirement of ~50 dpa.

This presentation outlines the major progress of the CFETR design during the past two years, including physics and engineering designs. The rest of the paper is organized as follows: section 2 focuses on the CFETR physics design, which mainly concerns the development of steady-state and hybrid operating scenarios by using the system code and integrated modelling tools, optimization of the divertor and impurity effects, and evaluation of the MHD stability and VDE controlling. Section 3 emphasizes the CFETR engineering design of key components, including the magnets, VV, tritium breeding blanket (TBM), divertor, and remote handling (RH). The summary goes into the final section.

2. CFETR physics design

The CFETR physics design mainly focuses on the development of the operating scenarios and their optimizations with respect to the physics and engineering constraints. The developed operating scenarios by a series of calculation and simulations will be used to predict the fusion performance, to explore and determine a robust operation space possessing good confinement, and MHD stability, to evaluate and limit the fraction of helium and other impurity particles while approaching the desirable fusion performance, to size up the compatibility of the power and particle exhaust with the chosen divertor configuration, to assess and manipulate the transit and steady heat load to the first wall and divertor to keep the machine safety. In the CFETR physics design, the system optimizer general atomics system code (GASC) [2] based on a Microsoft Excel spreadsheet, is used as the 0D system code to scope out the parameter space due to various operating modes [3–5]. The models in the 0D system code are either empirically or physics based but with simplifying assumptions. It can provide the zeroth order engineering parameters for further physics and engineering designs. In addition, the 0D system code can provide a consistent set of dimensionless parameters including $H_{ITER98Y2}$, β_N, f_{BS}, and q_{95}. Those parameters align themselves with fusion production, for example, fusion power and fusion gain, and give a ballpark estimate of fusion power production as well. However, the plasma performance generated by the 0D system code does not identify any realistic operating scenarios, even though the models in the code are based on the achieved experimental database and conservative extrapolations, since the strong interplay between the core transport, pedestal structure, current profile, and plasma equilibrium in the fusion reactor like CFETR should introduce some uncertainties on the fusion performance. To be able to accurately predict the fusion performance in a reactor, a proper way to simulate the plasma performance by using the physics-based integral models with parameters that are beyond the available experimental scaling laws. The integrated modelling is expected to be capable of calculating a self-consistence solution to the strong coupled problem and thus to benchmark the plasma performance predicted by the 0D system code [6]. Its prediction capability has been illustrated by reproducing the experimentally demonstrated scenarios. The automated

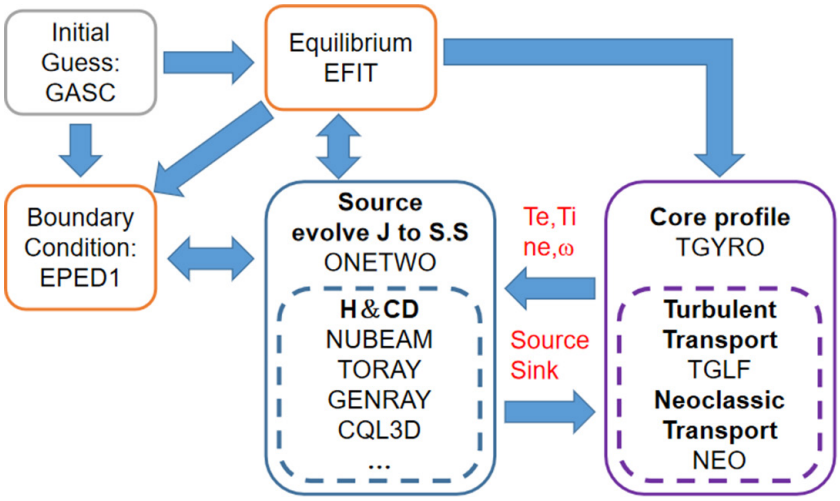

Figure 2. Workflow and the code suites in the OMFIT framework.

framework OMFIT [27, 28] is applied to physically integrate a couple of multi-dimensional code suites to perform the self-consistent simulations of the plasma core and pedestal, and then to provide a self-consistent solution for the CFETR transport, equilibrium and pedestal dynamics. Within this process, the predicted information about the CFETR fusion performance can be extracted. In the framework, several multi-dimensional code suites are involved, as shown in figure 2. The 1D transport code TGYRO [29] is used to solve the nonlinear problem to characterize the plasma performance in the core region. The physics-based models TGLF (i.e. toroidal gyro-Landau fluid model, which is a turbulent transport model) [30, 31] and NEO (which is a drift-kinetic neoclassical transport code) [32] engaged in the TGYRO are used to evaluate the turbulent and neoclassical transport, respectively. The pedestal model EPED1 [33] is used to provide the pedestal structure (e.g. width and height) based on the 0D system code output parameters. The TGYRO can provide a unique set of the plasma profiles that can make the transport flux match the volume integral of the summary of the sources and sinks. The sources (particles, energy, momentum) and sinks (radiation loss) as well as plasma current evolution are computed by the code suite ONETWO [34]. The models engaged in ONETWO are the ray-tracing codes TORAY-GA [35], TORLH [36], and TORIC [37] for the RF H&CD scheme, and the Monte Carlo code NUBEAM [38] for the neutral beam injection (NBI). In the integrated modelling, the NUBEAM is run stand-alone over an enough long time for collisional relaxation, and 10 000 markers are used to yield the converged current profile and heating profile. With the output evolution of pressure gradient and current gradient from ONETWO, the code EFIT [39, 40] can be employed to update them and provide the close boundary equilibrium.

To predict the fusion performance of the specified CFETR operation scenario, the integrated modelling starts with the inputs from the 0D system code estimation, then iterates among transport, equilibrium and pedestal, and evolves the particle densities, T_e, T_i and momentum toward the specified operating scenario. Consistently, the auxiliary power for heating and current drive is adjusted to keep the specified scenario operating. In the iteration, the SOL solution should match the core parameters at the pivot point (about $\rho \sim 0.9$), which is located at the top of the pedestal. Along with the operating scenarios developed within the OMFIT framework, the time-dependent simulation of the plasma performance in different phases of the discharge, including flattop, ramp-up, and ramp-down, are carried out by tokamak simulation code (TSC) with some auxiliary heating subroutine packages [7]. The TSC is a full non-linear free boundary simulation code that accurately models the transport time-scale evolution of an axisymmetric plasma, including the plasma interactions with the passive and active feedback systems.

With the GASC output parameters and integrated modelling workflow, two CFETR operating scenarios, fully non-inductive (or steady-state) and hybrid mode, are calculated and given below. Verifications of codes and the model used in the workflow are being performed especially, including the improvement of the TGLF transport model in recent years [8]. Independent verifications of the developed CFETR scenarios by integrated modelling using codes developed in Europe such as METIS [41], CRONOS [42] and others are also started.

2.1. Development of fully non-inductive and hybrid mode scenarios

Table 1 illustrates the calculated 0D key parameters for a fully non-inductive (steady-state) operating scenario developed for the CFETR with the fusion power P_f ranged from 100 MW to the DEMO level of >1 GW. As listed in table 1 for Cases A.1 to A.3, the parameters are reasonable, either based on the achieved experimental database or conservative extrapolations. The Z_{eff} is prescribed to be 2.45 in the system code study. It is perceived that the CFETR fusion energy production ranged from 100 MW to ~1 GW can be achieved by having a proper confinement factor $H_{ITER98y2}$ (1.12–1.41), moderate normalized β_N (1.0–2.0) and a fraction of bootstrap current f_{bs} (less than 50%). By increasing the normalized β_N from 1.0 to 2.0, the steady-state scenarios with fusion power production of 100 MW, 200 MW, 500 MW and 1 GW are obtained, respectively. For $P_f \leqslant 1$ GW, β_N keeps at low level.

Table 1. CFETR plasma performance for CFETR fully non-inductive (steady-state) oparating scenarios.

CFETR fully non-inductive $R = 7.2$ m, $a = 2.2$ m, $\kappa = 2$	Parameters	A.1 100 MW	A.2 200 MW	A.2 500 MW	A.3 1 GW	A.4 DEMO-level
Fusion power (MW)	P_f	120	229	482	974	2192
Power to run plant (MW)	$P_{internal}$	199	196	223	238	265
Gain for whole plant	Q_{plant}	0.46	0.70	1.14	1.98	3.79
Pfusion/Paux	Q_{plasma}	1.56	3.06	5.87	11.89	28.17
Net electric power (MW)	$P_{netelec}$	−107	−58	30	232	738
Neutron power at blanket (MW m^{-2})	P_n/A_{wall}	0.12	0.23	0.49	0.99	2.23
Toroidal beta	β_T	0.006	0.009	0.014	0.019	0.029
Normalized beta	β_N	1.00	1.20	1.50	2.0	3.0
Bootstrap fraction	f_{bs}	0.40	0.40	0.40	0.50	0.75
H factor over ELMY H_net	$H_{ITER98Y2}$	1.12	1.25	1.32	1.41	1.42
Ohmic fraction	f_{ohm}	0.0	0.0	0.0	0.0	0.0
Current drive power (MW)	P_{cd}	77	75	82	82	78
Plasma current (MW)	I_p	8.61	10.34	12.92	13.78	13.78
Field on axis (T)	B_T	6.5	6.5	6.5	6.5	6.5
Ion/electron temperature (keV)	$T_i(0)/T_e(0)$	18	24	32	36	32
Electron density (10^{20} m^{-3})	$n(0)$	0.48	0.52	0.61	0.78	1.31
Ratio to Greenwald limit	n_{bar}/n_{GR}	0.57	0.51	0.48	0.57	0.96
Zeff	Z_{eff}	2.45	2.45	2.45	2.45	2.45
Transport power per unit R (MW m^{-1})	P_{SOL}/R	8.52	9.42	11.66	15.69	30.70
q95_iter [2]	q_{95_iter}	8.87	7.39	5.91	5.54	5.54

Thus, the challenges for material, heat exhaust, plasma disruption and plasma wall interaction are relatively weaker compared with the ITER. Efforts will be focused on the tritium breeding. If β_N is fixed at ~3, DEMO-level parameters with the fusion power ~2 GW would be even achieved. This 0D table is used to guide more complex physics modelling and the coupled design activity between physics design and engineering design.

A preliminary integrated simulation is performed to establish the operating scenario to verify the 0D calculation of the P_f ~ 1 GW as given in table case A.3. In the simulation, the auxiliary heating and current drive (H&CD) scheme is chosen to the combination of EC and NBI [9, 10]. The electron cyclotron wave (ECW) is launched from the top used to improve the current-drive efficiency. The ECW power is about 30 MW operating at fundamental O mode with the frequency of 250 GHz, applied to drive ~0.88 MA to maintain the magnetic shear in the core and to control $q_{min} > 2$ to avoid any low n MHD mode instabilities that might lead to disruptions. Further optimization of EC wave frequencies, launch position, poloidal injection angle and toroidal injection angle is needed to improve the CD efficiency and fusion performance. A two NB injector scheme is employed here, one has the beam power of 68 MW, beam energy up to 500 keV, injection tangential radius $R_T = 830$ cm, used to drive the current up to 4 MA, while the other beam has the beam power of 10 MW, a slightly lower beam energy, 100 keV, $R_T = 7.2$ m is used to drive the plasma rotation at the edge to improve confinement leading to higher temperatures, thus a higher fusion gain. In the optimization of the NBI scheme, the launch angle should be chosen to avoid both large shine through and edge heating and also to enhance the current drive, and NBI port size would be as small as possible for saving more mid-plane space for tritium breeding blankets. The bootstrap current from the NEO model is about 7 MA. Some key parameters for fusion power production up to 1 GW predicted by integrated modelling (0D calculation) are $H_{ITER98y2} = 1.1$ (1.41), $\beta_N = 2.4(2.0)$, and f_{bs} ~ 59.5% (50%). The total current in this scenario is about 12 MA, which has a very high edge safety factor that would benefit to the plasma stability. The equilibrium and current (q) profiles are shown in figure 3. Figure 3(a) depicts the various components of the plasma current. Figure 3(b) shows the q profile, which has a strong negative central magnetic shear (NCS), since the scenario generates a large off-axis bootstrap current as shown in figure 3(a) due to the strong NB heating. It is noted that the ohmic current is close to zero in the integrated modelling result, which demonstrates a steady state is approximately reached. In addition, a higher β_N together with a higher q_{95} (~5.8, due to a higher B_T and lower I_p) enables a higher bootstrap current fraction of 59% compared to the 50% assumed in the 0D analysis.

Table 2 shows the CFETR plasma performance for the hybrid mode operating scenario. For Cases B.1 ($P_f = 100$ MW) to B.3 ($P_f = 1$ GW) as listed in the table, some key parameters are almost the same as the steady-state scenarios but $H_{ITER98y2}$ is slightly lower.

The hybrid mode operating scenario is also considered, aimed to maintain the pulse length to 8 h. The pulse length is about two times the tritium recycling time, thus the tritium self-sufficiency can be tested under the hybrid mode operating scenario. The integrated simulation is also performed to establish the hybrid mode operating scenario to verify the 0D calculation given in table 2 case B.3. It is worth noting that the simulating results are approximate in qualitative as the 0D predictions, except the H&CD power needs 103 MW from the simulation and is larger than 74 MW from the 0D calculation,

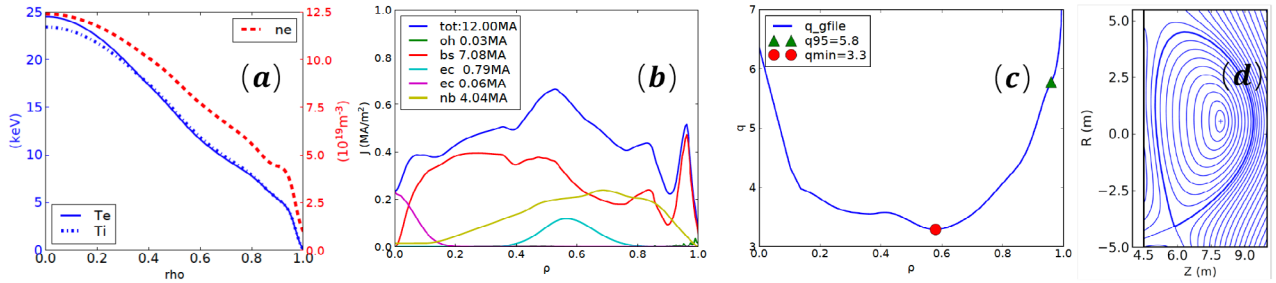

Figure 3. (*a*) Temperature profiles, (*b*) current profile, (*c*) *q* profiles, (*d*) equilibrium for the fully non-inductive scenario by integrated modelling as given in of table 1 case A.3. The abscissa ρ represents the normalized square root of toroidal magnetic flux. In the legend of (*b*), 'tot', 'oh', 'bs', 'ec', 'nb' represent the profiles of the total current, the ohmic current, the boostrap current, the EC driven current and the beam driven current, respectively.

Table 2. CFETR plasma performance for CFETR hybrid mode oparating scenarios.

CFETR hybrid mode $R = 7.2$ m, $a = 2.2$ m, $\kappa = 2$	Parameters	B.1 100 MW	B.2 200 MW	B.2 500 MW	B.3 1 GW	B.4 DEMO level
Fusion power (MW)	P_{f}	114	250	558	1128	2192
Power to run plant (MW)	P_{internal}	190	196	202	222	75
Gain for whole plant	Q_{plant}	0.46	0.75	1.40	2.41	12.96
Pfusion/Paux	Q_{plasma}	1.54	3.35	7.65	15.30	795.16
Net electric power (MW)	P_{netelec}	−103	−49	80	312	891
Neutron power at blanket (MW m^{-2})	$P_{\mathrm{n}}/A_{\mathrm{wall}}$	0.12	0.25	0.57	1.15	2.23
Toroidal beta	β_{T}	0.006	0.009	0.014	0.019	0.029
Normalized beta	β_{N}	1.00	1.20	1.50	2.00	3.0
Bootstrap fraction	f_{bs}	0.40	0.40	0.40	0.50	0.75
H factor over ELMY *H*_net	H_{ITER98Y2}	1.01	1.09	1.18	1.19	1.54
Ohmic fraction	f_{ohm}	0.30	0.30	0.30	0.30	0.24
Current drive power (MW)	P_{cd}	74	74	73	74	3
Plasma current (MA)	I_{p}	8.61	10.34	12.92	13.78	13.78
Field on axis (T)	B_{T}	6.5	6.5	6.5	6.5	6.5
Ion/electron temperature (keV)	$T_{\mathrm{i}}(0)/T_{\mathrm{e}}(0)$	13	17	24	24	34
Electron density (10^{20} m^{-3})	$n(0)$	0.67	0.74	0.82	1.16	1.23
Ratio to Greenwald limit	$n_{\mathrm{bar}}/n_{\mathrm{GR}}$	0.79	0.72	0.64	0.85	0.90
Zeff	Z_{eff}	2.45	2.45	2.45	2.45	2.45
Transport power per unit *R* (MW m^{-1})	P_{SOL}/R	7.58	9.33	12.63	19.11	22.97
*q*95 iter	q_{95_iter}	8.87	7.39	5.91	5.54	5.54

which leads to a lower fusion gain. And the confinement is also lower; H_{ITER98y2} is only 1.06 compared to the 1.19 predicted by the 0D code. The integrated modelling reveals that the CD power chosen in the 0D code is not sufficient to reach the target temperature and confinement when physics-based transport is taken into account in the integrated modelling. In the simulation, the H&CD scheme is chosen to the combination of NBI, ECW, low hybrid wave (LHW) and/or fast wave (FTW). The ECW is launched from the top and LHW (or FTW) is launched from the high-field side (HFS), both of them are used to drive the current. In this simulation, the ECCD power is about 30 MW, operated in the fundamental frequency of 250 GHz while the LHW with the frequency being 4.6 GHz (or FTW with the frequency being 1.4 GHz) power is about 20 MW. The frequencies and the injected spectrum/angles are chosen based on scanning studies with ray-tracing codes, as discussed in [10]. The current driven by the RF waves is about 2.22 MA, used to produce a broad *q* profile with the q_{min} slightly larger than 1 and to maintain a weak magnetic shear in the core region, which can prevent the sawteeth and thus, to avoid the triggering of neoclassical tearing mode (NTMs, e.g. $m/n = 2/1$ and 3/2) instabilities, and to access possible improved confinement at higher β_{N}. The two NBI injectors scheme with power up to 52.6 MW is used, one has the beam energy up to 600 keV, $R_{\mathrm{T}} = 660$ cm, used to drive the current (~1.53 MA), the other beam has slightly lower beam energy, 300 keV, $R_{\mathrm{T}} = 420$ cm is used to drive the plasma rotation at the edge to improves confinement. Such composition enables the sharing of a window by two beams and avoids the on-axis current drive breaking the flat or weak shear safety factor profile. Similar to the fully non-inductive operation scenario, further optimization of the NBI scheme and ECCD is also needed. In this scenario, the ohmic current is about 30% of the total current, resulting in continuous consumption of the flux swing, which leads to a long pulse operation. Figure 4 demonstrates the hybrid mode operation scenario for the CFETR 1 GW mission. Figure 4(*a*) is the electron density, electron temperature, and ion temperature profiles. The temperature

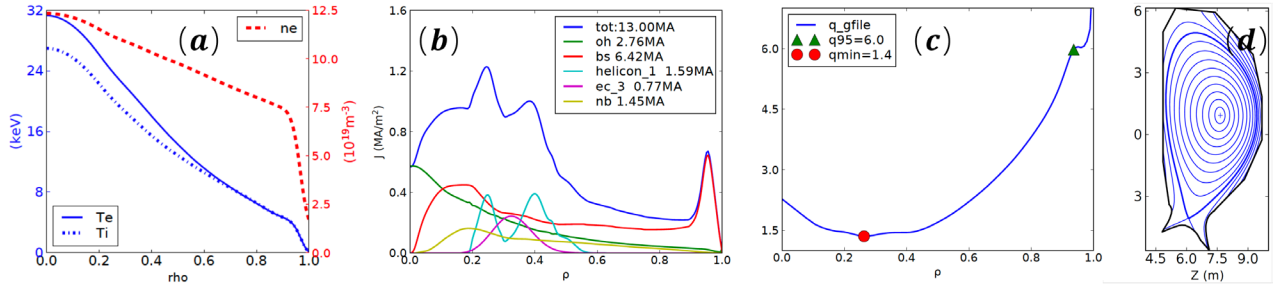

Figure 4. (*a*) Temperature profiles, (*b*) current profile, (*c*) *q* profiles, (*d*) equilibrium for the hybrid mode scenario by integrated modelling as given in of table 2 case B.3.

profiles have the steep shape in the core region, which contributes a large amount of bootstrap current. Figure 4(*b*) plots the various components of current profiles, the bootstrap current calculated by the Sauter model is about 50.5%, much less than that value in the fully non-inductive scenario, mainly due to the NB heating in the core region. The ohmic current is about 2.7 MA, indicating that the scenario is a hybrid mode operation. Figure 4(*c*) is the corresponding total current and q profiles, it has a slightly negative magnetic shear in the core, and $q_{\min}$ just above 1, also indicating that it is the hybrid mode operation. Figure 4(*d*) contours the predicted equilibrium configuration in a cross-section of the CFETR.

It is worth noting that in both operation modes, the plasma current is chosen to be much lower, correspondingly, the edge safety factor can be much higher benefiting for long pulse operation and disruption avoidance, and the need for auxiliary heating and current drive power tends to be less.

2.2. Consideration and optimization of the divertor configuration and impurity effects

The lower single null divertor configuration, similar to that of the ITER, is proposed for the CFETR design. The CFETR divertor will be located in the lower part of the vacuum vessel to remove the particles (including helium and impurity content) from the plasma core and to exhaust major part of the plasma thermal power. Especially, the capability of the divertor to exhaust the plasma thermal power is a critical issue to the successful and safety operation of a fusion power reactor. The heat load to the divertor can be evaluated by the figure of merit as the fusion power per unit major radius (P_{SOL}/R). As indicated in tables 1 and 2, P_{SOL}/R can reach 15.69 or 19.11 MW m^{-1} with respect to either fully non-inductive or hybrid mode operation for the CFETR $P_{\mathrm{f}} = 1$ GW mission, but technologically the maximum stationary heat flux, which can be extracted by the divertor is limited to 10 MW m^{-1} at present [11]. Therefore, the divertor heat load has to be controlled for CFETR long pulse or steady state operation. Further optimization of the divertor geometry, for example, expanding the field lines approaching the divertor target surfaces and shaping the surfaces to reduce the perpendicular heat flux is needed.

Since the plasma shape has a close relationship to the divertor geometry, it can affect the plasma performance in the divertor region. For example, the larger the plasma triangularity is, the smaller the divertor volume on the high field side.

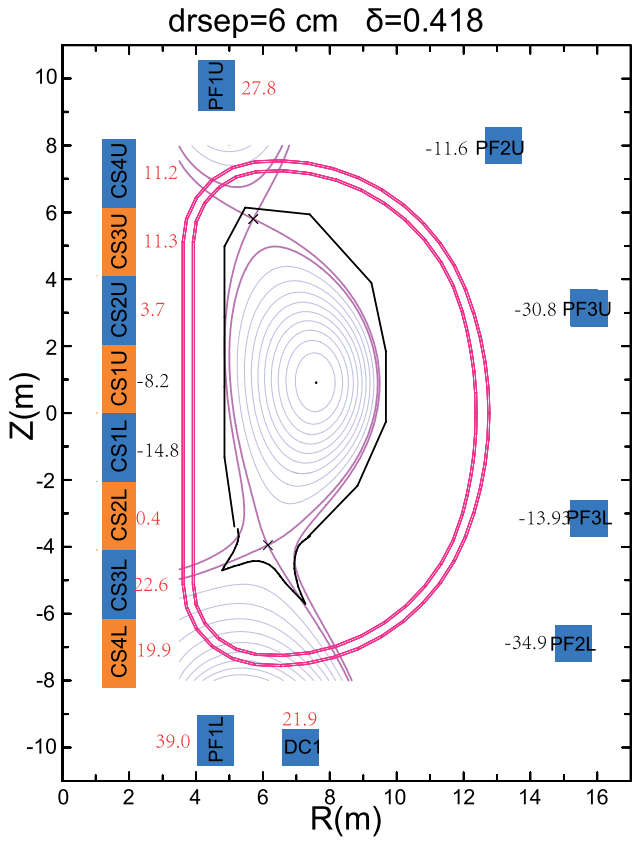

Figure 5. The reference equilibrium of the ITER-like configuration for the CFETR.

It will give restriction to the radiation in the divertor region and thus affect the plasma detachment yielded. Therefore optimization of the position of the X-point and the divertor strike point along with a proper plasma shape is definitely needed. Based on the 0D parameters, using the equilibrium code TEQ in CORSICA [43], sequences of equilibria with different triangularity (range of 0.3–0.8) are constructed. Through the iterations with the structures of the divertor and blanket, the reference equilibrium of the ITER-like configuration for CFETR with an acceptable position of the X-point and divertor strike point can be obtained, as shown in figure 5, which has the triangularity $\delta_{\mathrm{upper}} = 0.390$, $\delta_{\mathrm{lower}} = 0.446$ and $\mathrm{d}R_{\mathrm{sep}} = 6$ cm. This equilibrium is used as the start point for many design works. Besides the standard divertor configuration, the snowflake + (SF+) divertor configuration has also been considered. Calculations showed that the SF + is

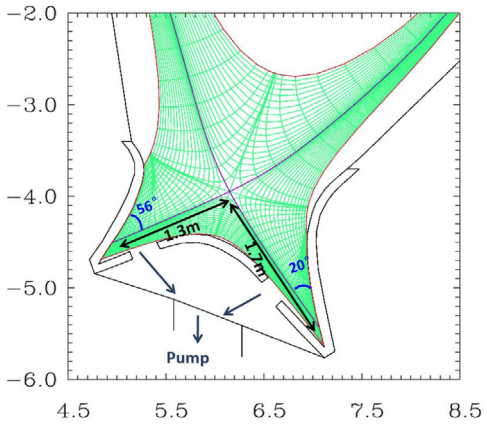

Figure 6. ITER-like divertor geometry and simulation mesh for the SOLPS code.

compatible with the standard divertor and the current in the PF coils is below the engineering limit. As already discussed in the previous design [1], by using extra superconducting coils (DC1) together with other PF coils, either the X-divertor or snowflake advance divertor configuration can be realized with field expansion of 1.5–4 times.

At present the divertor physics design focuses on the ITER-like divertor based on the steady state scenario described in section 2.1. We integrated the requirements for the magnetic configuration, blanket and the space limitations. The exhausted thermal power from the core plasma is expected to be ~300 MW, which includes the heating power that the fusion plasma produces and supplied externally, needed by the current drive for steady-state operation. Since the wetted surface is expected to be ~3 m^2 at the target for CFETR, this will result in a high power density ~100 MW m^{-2} at the targets. However, the current limits on perpendicular heat flux to actively cooled tungsten divertor target structures are typically 10 MW m^{-2} in steady state and up to 20 MW m^{-2} during transients [11]. To reduce the peak power density, the divertor target is inclined with a poloidal angle between the outer leg and the outer target plate ~20°. A longer outer leg (~1.7 m) than the inner one has been used to increase the divertor volume for higher radiation in the outer divertor region, since higher power is transported into the outer divertor than the inner one. A V-shape design in both targets can enhance neutral accumulation. The pumping slot of the divertor cassette is located at the bottom, similar to the ITER. A larger inclined angle at the inner target (~56°) can increase the reflection of neutrals towards the outer divertor and to facilitate the buildup of neutrals around the pump slot for higher pump efficiency. The divertor structure is shown in figure 6.

The integrated divertor simulation code, SOLPS [44], has been applied to the CFETR divertor design. The SOLPS simulation can help to optimize the divertor geometry and find a solution for edge power handling. Impurity seeding has been considered as a primary technique to increase the radiation loss in the edge and divertor such as ITER [12]. The preliminary modelling results show that high radiation loss in edge ($f_{rad} > 80\%$) is required to handle large power. However, fuelling dilution and fusion performance degradation in the core region should be carefully concerned for the high radiation scenarios. Further optimization like a small-angle slot configuration (SAS) [13] and long leg divertor is still ongoing. Additionally, snowflake configuration with a larger magnetic expansion factor will also be evaluated and compared in future.

Another key aspect of the solution is the choice of plasma-facing materials for the divertor manufacture. Similar to the ITER, tungsten (W) is used to cover the divertor surfaces, which endorses the divertor with some favourable characteristics, for example, the highest melting point of any metal, and an acceptably low affinity for hydrogen, implying a low rate of fuel retention. However, we have to take some measures to avoid excessive concentrations of tungsten accumulating in the plasma core. The simulation results [14] indicate that when the fraction of tungsten impurity increases from 0 to 6×10^{-5}, the L-H transition power threshold $P_{L\text{-}H}$ increases slightly, but the radiation power P_{rad} rises dramatically, which would lead to a further drop of the P_{transp} (where $P_{transp} = P_{NB} + P_{EC} + P_{alpha} - P_{brem}$ [24]), even though the fusion performance only has a slight declination. When the W concentration reaches 4×10^{-5}, $P_{transp} < P_{L\text{-}H}$, the plasma confinement drops back to the L-mode. It is concluded that the tungsten impurity tolerance is limited by $P_{transp} > P_{L\text{-}H}$ if we want to keep the plasma staying in the H-mode. The other key point is how to avoid helium dilution when a large amount of fusion reactions occur in the plasma core, which can reduce the fusion performance. A study of the trend of helium dilution on a steady-state scenario by varying the fraction of helium ash from 0.05 to 0.2 [15] shows that when the helium fraction increases, the CFETR fusion performance ($H_{ITER98Y2}$, Q, f_{bs} and τ_E) decreases gradually. As the helium dilution fraction reaches 0.2, the fusion gain Q drops below 1. Therefore, necessary precautions to enhance the helium transport from the plasma core to the divertor and to move the helium ash out of the divertor are a critical issue in the design of the divertor pumping capability.

Externally impurities in the core, which have less negative impacts on the plasma core performance, would help partially radiate the heat before it reaches the divertor. Since impurity will raise Z_{eff}, a scan of Z_{eff} by varying concentrations of argon (Ar) seeding based on an optimized fully non-inductive steady-state scenario has been performed to look for the achievable maximum core impurity radiation without degrading or affecting the core plasma performance less. As shown in table 3, when Z_{eff} increases, the fusion performance ($H_{ITER98Y2}$, Q, f_{bs}, τ_E) increases before dropping off as Z_{eff} reaches the turning point of 2.78. Further analysis of transport for these cases shows that low-k ion temperature gradient (ITG) modes dominate the turbulence. The decrease in linear growth rate and resultant fluxes of all channels with increasing Z_{eff} can be traced to the change of impurity profile by transport. And the improvement levels off at a higher level. Therefore, there is a competition between the suppression of turbulence and increasing radiation loss along with the increasing Z_{eff} results in the peak values of the fusion performance as verified in the table. At the turning point, the P_{LOSS} can reach a fraction of 25.7% of the total power. Since the

Table 3. Impurity effects on fusion performance by varying Z_{eff}.

Z_{eff}	P_{LOSS}/P_{TOT} (%)	$H_{ITER98Y2}$	Q	f_{bs} (%)	τ_E (s)
1.52	12.7	0.86	1.44	35.5	1.48
1.89	17.1	0.92	1.61	37.2	1.60
2.11	19.6	0.96	1.76	39.6	1.66
2.35	21.8	0.98	1.75	40.3	1.68
2.78	25.7	1.01	1.76	42.1	1.76
3.20	29.5	1.00	1.58	42.3	1.78
3.67	34.4	1.00	1.44	43.7	1.78

impurity can lower the current drive efficiency by ECW, more additional power is required to maintain steady state operation. It is worth noting that the simulation is not very sensitive to the assumed impurity profile. This finding is encouraging as part of the divertor heat load solution.

2.3. The MHD stability of the developed scenarios

The development of the CFETR operation scenarios not only has to take into account some engineering constraints as power and particle exhausts, etc, but also needs to satisfy all the requirements of plasma confinement and stability physically. It is conceivable that in a burning plasma of a fusion reactor like CFETR, access to confinement somewhat better than the standard H-mode level is required to achieve significant fusion gain. However, to sustain such a high fusion power under stationary conditions over the specified plasma scenarios definitely requires sophisticated control of the core, edge and divertor plasma conditions to avoid the degradation of core plasma conditions and any dangerous MHD instability, which may lead to plasma disruption. For example, the CFETR fully non-inductive operation will explore a more complex plasma regime in which the total plasma current is driven by a combination of auxiliary heating power driven current and bootstrap current, which would trigger some undesirable instabilities. Therefore, the current profile shape needs to be controlled to maintain MHD stability [25]; to some extent the active feedback control of certain MHD instabilities may also be required. The MHD behaviours with respect to the developed CFETR operation scenarios below the no-wall Troyon limit are given in figures 5 and 6 of [16] (for the previous small-size design with the major radius being 5.7 m and fusion power being 200 MW). It is found that the dangerous low-n modes can be stabilized by the wall at $r/a = 1.2$, but some unstable modes at the plasma edge can be driven by the strong pedestal gradient. Figure 2 of [16] demonstrates that the developed scenarios can be operated in a broad range of β_p and β_N in the region constrained by two limitations that are denoted by two black lines due to current limit and the unstable modes. Further studies targeting the operation scenario with a larger major radius and higher density and lower edge temperature suggest that the CFETR might operate in a grassy ELM regime or QH modes, as indicated in figure 15 of [23]. In the figure, a mix of grassy ELM and type I ELMs can be identified, and the grassy ELM can occur when the collisionality is ranged from 0.1 to 1 and β_p ranged from ~1.6 to ~2.8. The CFETR operating in the grassy ELM region would not only benefit to the MHD stable, but also to reducing the heat load to the divertor target. However, more experimental data is needed to test the scaling. Another challenge here is how to access to the QH mode regime. Similar analysis is being extended to the present design (with the major radius being 5.7 m) especially for high fusion power scenarios close to or beyond the Troyon limit. It is well known that edge harmonic oscillation (EHO) is a key issue in QH operation [26]. The peeling ballooning boundary of CFETR is given by the parameter scan with EPED. And based on figure 10 in [17], linear and nonlinear characteristics of instability near the peeling boundary is under progress with BOUT + +.

Experimental and theoretical studies have confirmed that plasma elongation can increase the achievable plasma current, density, plasma beta and fusion plasma performance. However, elongated plasmas are inherently vertically unstable. Therefore vertical stabilization analysis is of great importance for the CFETR design. The vertical displacement events' (VDEs) stabilization analysis is conducted within vacuum vessel and blanket modules (BMs) by employing the TokSys and TSC tools. TSC [22] is a fully non-linear free boundary simulation code that accurately models the transport time-scale evolution of an axisymmetric plasma, including the plasma interactions with the passive and active feedback systems. The TokSys [23] RZIP model is a linear model that treats the plasma as a fixed spatial distribution of current, and rigid radial and vertical motions are allowed. Both of them are the widely used 2D simulation codes. They have been successfully used on several tokamaks in reproducing experimental VDE shots and/or designing vertical control, such as PBX, DIII-D, TFTR, JT-60U, and EAST. The TokSys RZIP model is a linear model that treats the plasma as a fixed spatial distribution of current, and rigid radial and vertical motions are allowed.

The double layer VV and the BMs are considered the main passive stabilizers for the CFETR VDE control. Both the TokSys and TSC codes treat the passive conductors as a group of toroidal continuous filaments with neither breaks nor shunts. Equivalent resistivity is derived from the total resistance of the VV. The structure wall of the blanket module breeding zone is equivalent to a conductive shell, together with the manifold and back support structure at the rear of the blanket module becoming a conductive body. The volume composition of RAFM steel (e.g. CLF-1) used in the conductive shell, the manifold and the back support structure is 71.1%, 45.3% and 87.3%, respectively. The resistivity of the CLF-1 steel in 300 °C is $7.62 \times 10^{-7}\ \Omega \cdot \mathrm{m}$. This value is used for the BMs' conductor resistance computation. The field penetration time (L/R time) for various toroidal mode numbers of passive stabilizers are shown in figure 7. Eigenvalues of VV only and VV&BM are computed. The first-order eigenmode is the even symmetry mode which has the largest L/R time, mainly for plasma radial control. For VDE control, the odd symmetry modes play a key role, of which the second-order eigenmode, which has the large L/R time, corresponds to the main vertical stabilization. Applying the equilibrium as given in figure 5, the growth rates of VDE can be computed with respect to the specified

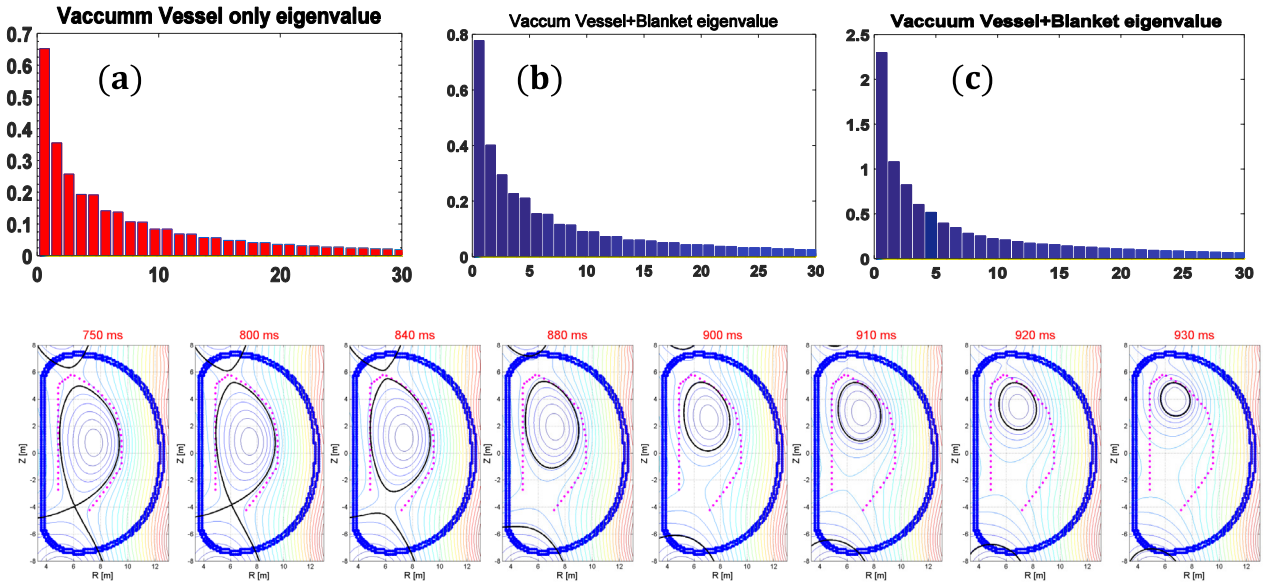

Figure 7. *L*/*R* time versus toroidal mode number for (*a*) VV, (*b*) VV&BM (original resistance) and (*c*) VV&BM (original resistance times 10). Here *X*-axis denotes the toroidal mode number, while the *Y*-axis is the *L*/*R* time (s).

conductor structures (VV or VV + BMs). It is found that only when VV is considered as the passive stabilizer, VDE is uncontrollable. With both VV and BMs, growth rates of VDEs are limited to small ones, but non-zero. VDE growth rate is 2.2 when the BM original resistance (multiplier equals 1) is used. The growth rate increases to 18.1 when the original resistivity multiplies by 10. That means the BMs have a strong passive stabilization effect on VDEs, but the internal coils (ICs) are still necessary to control the VDE. The ICs should be installed behind the blanket. It is still under assessment.

Figure 7 shows the plasma evolution, simulated by TSC. After initial equilibrium construction, all the feedback controls are shut down and only the VV passive stabilization effect is considered. The plasma freely drifts vertically until un-convergence occurs. Further analysis shows the growth time of the VDE is about 2 ms, which is much less than the field penetration time (>400 ms) given in figure 7(*b*). It is evident that besides the VV structure, other passive structures are necessary to enhance the vertical stabilization capability to lower the shift caused by the VDE.

The MHD instabilities driven by energetic particles are important issues. Preliminary work has been carried out for the steady-state scenario, to study the impact of fast ions, which are born of the D–T alpha particle and the NBI. The work is performed with the NOVA-K [45], NIMROD [46] and AWEAC codes [17]. As the first step, the linear instabilities of the toroidal Alfven eigenmode (TAE) and reversed shear Alfven eigenmode (RSAE) are analysed [47]. Both NOVA-K and NIMROD show that the alpha particle can drive TAEs and RSAEs very weakly. The reason is that the AE gaps are narrow at the central region, where alpha particles are concentrated. While the NBI fast ion cannot drive the instabilities, since the corresponding β_{beam} is relatively low. NOVA-K also calculates the rates of Landau damping, radiation damping and collision damping, which shows that the Landau damping dominates. These driving and damping effects make the TAEs and RSAEs marginally stable. Thus, the linear AEs will not be a concern. The effects of nonlinear AEs and EPMs are still under investigation.

3. CFETR engineering design

Currently there are eight tasks for the CFETR infrastructure design, namely layout design and system integration, superconducting magnet and cryogenics, vacuum vessel & vacuum system, in-vessel components, standardization and design management, heating & current drive system, diagnostics & CODAC, remote maintenance system. In this section, progress of some of the eight tasks in the last two years is presented. In addition, many R&D activities have been carrying out in order to verify some advanced design as well as to exploit some key technologies for the critical components.

3.1. Magnet system

The requirement for sustaining long burn duration as specified in the duty time CFETR mission necessitates the use of superconducting magnets. Several major magnet systems are involved in producing the required magnetic field configuration and in generating the high plasma current (up to 14 MA) necessary to confine the burning plasma: the 16 toroidal field (TF) coils, 8 central solenoid (CS) modules, 6 poloidal field (PF) coils, and 18 correction coils (CC). We focus mainly on the progress of the CS coils, TF coils and the R&D activities of the superconducting coils in this section.

To meet the requirement of the CFETR mission, the 16 TF D-shaped (six arcs and a straight leg) coils with a plasma major radius of 7.2 m are designed, as shown in figure 8. The TF coils totally have 168 turns. A high-performance superconducting magnet with advanced J_c (Critical current density) Nb_3Sn RRP (restacked-rod-process) superconducting strands

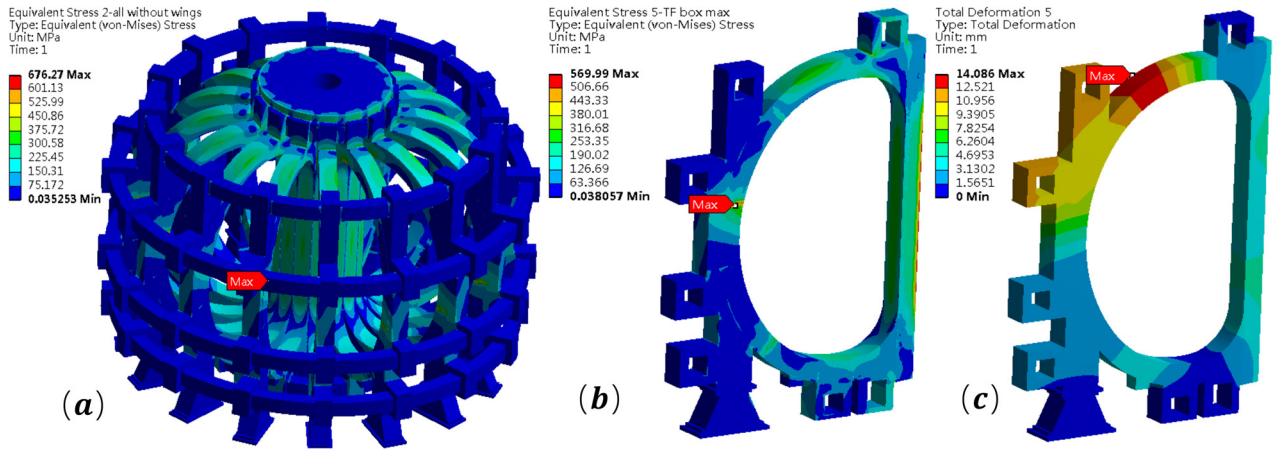

Figure 8. Stress analysis for (*a*) the whole TF system, (*b*) one TF coil, and (*c*) deformation of the TF conductor.

is used for the TF coils' fabrication. The detailed parameters of the conductor are introduced in [48]. The TF coils operate at a maximum (conductor) current of 84.6 kA to provide a toroidal magnetic field on the plasma axis of up to 6.5 T, with a maximum field in the inboard length of ~14 T. The current per turn and total storage energy (116.34 GJ) of CFETR TF are much larger than ITER-TF (40.1 GJ). The Nb_3Sn cable-in conduit conductors (CICC) with rectangular cross section are graded for TF coils to reduce the costs of the superconducting strands. The stress analysis of each TF coil has been done and the results are shown in the figure. It is evident that each TF coil will experience a centripetal force in the TF inner leg towards the main machine and the maximum force will reach ~570 MPa (figure 8(*b*)), and the maximum deformation of the coil can reach 14 mm. Therefore, nearly half of meter thickness of the coil-case is designed to resist the force.

Since the CFETR have another option to be run in hybrid mode, in order to provide the sufficient magnetic flux for driving the ohmic current and shaping the plasma, the CFETR central solenoid coils system, assembling from eight modules is designed to provide maximum 400 VS flux with a maximum rate of field swing of ~1.2 Ts over the device lifetime. The CS coils have a maximum radius of 2.25 m, which can also be seen in figure 1. Each module has 720 turns with the structure of 18 (horizontal) × 40 (vertical). Each module can be powered independently for plasma equilibrium requirements. The high temperature superconductor with Bi2212 material and low temperature superconductor of Nb_3Sn strands are used to generate a maximum magnetic field of 19.9 T at 51.25 kA/turn, as shown in figure 9. All coils are cooled with supercritical helium with a coil inlet temperature of 4.5 K.

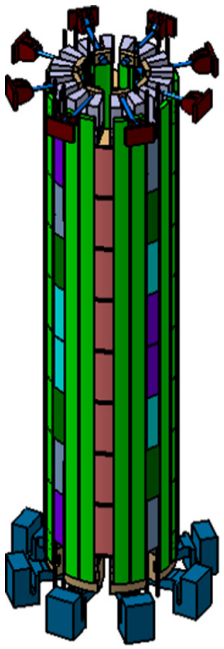

Figure 9. Perspective view of the CFETR CS.

3.2. Vacuum system

The whole CFETR vacuum system involves several large volume systems, including the cryostat, torus, and several lower volume systems. The vacuum vessel of CFETR is designed to be a toroidal chamber with an outside diameter of ~25.5 m and a height ~15 m which not only provides the high quality vacuum required for the plasma operation, but also acts as the first confinement barrier for the tritium & other fuels. The entire tokamak core is contained within a cryostat (~29 m diameter × ~38 m height, which has the background pressure ~10^{-4} pa). A series of stainless-steel thermal shields, cooled by 1.8 MPa pressurized helium gas from the main cryoplant with an 80 K inlet temperature, reduces heat transfer to the superconducting magnet systems.

The CFETR VV is designed to be a torus with a D-shaped cross-section, 16 upper vertical ports, 8 lower ports and 6 equatorial ports, as shown in figure 10. The inner, outer shells and stiffening ribs between them are joined by welding. To reduce the difficulty of the manufacture, the cross-section of the VV (D-shape) is made up of three arcs and one straight line segment, which are tangential to each other. Two VV shells are designed with 50 mm in thickness. The material of the VV is 316L(N)-IG. The four upper ports will be used for maintenance and disassembly of blanket. The six lower ports are for the divertor maintenance and the cryo-pumps. The eight equatorial ports will be used for NBI, the diagnostic and some remote handing (RH) tools. Considering the different neutron

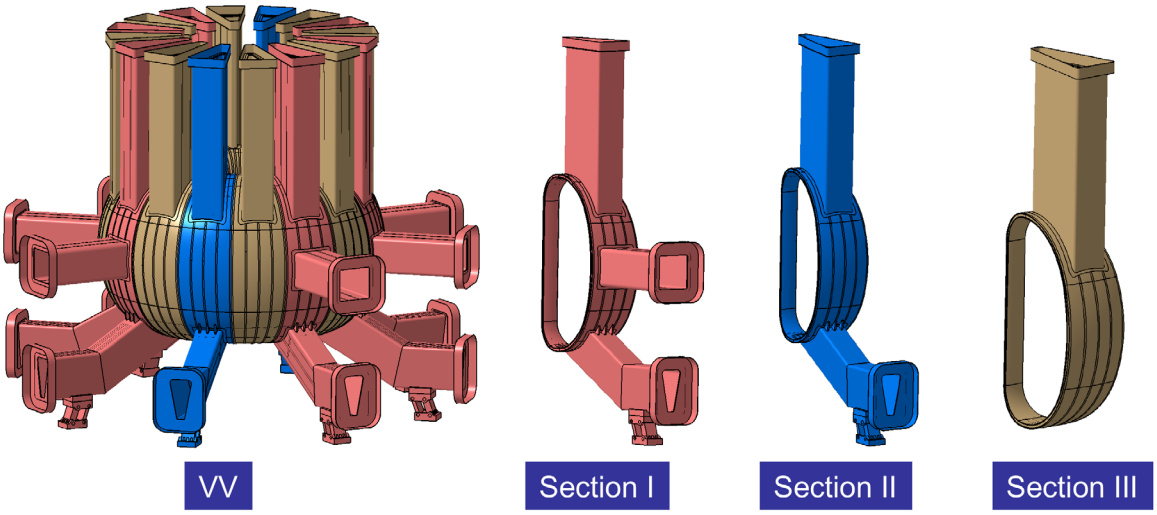

Figure 10. 3D model vacuum vessel for CFETR.

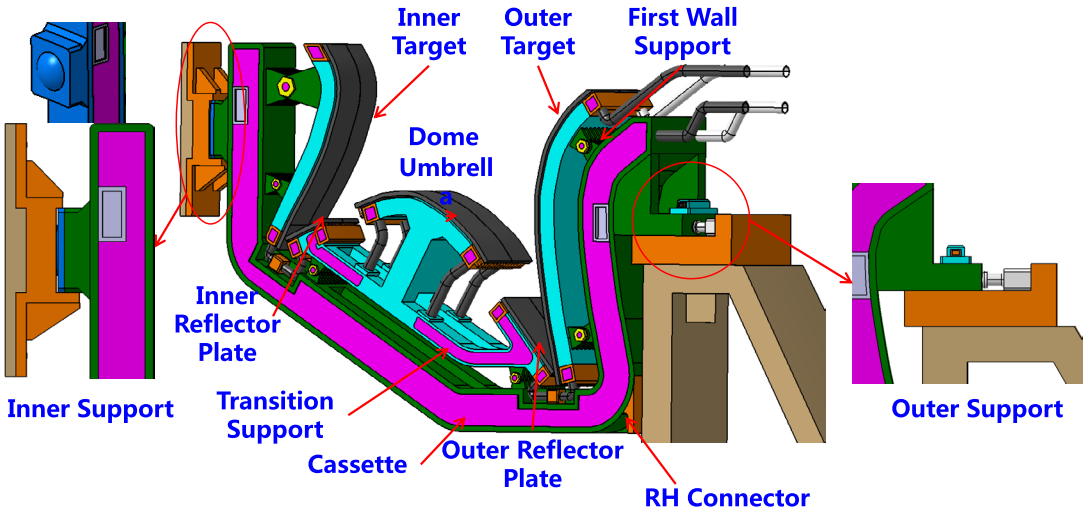

Figure 11. Conceptual engineering design of the CFETR divertor structure.

irradiation dose for the superconducting magnet coils, an unequal space between the double-walled structure at the inboard and outboard regions is adopted. From the VV inner shell to the boundary of the plasma, a radial dimension of at least 1000 mm is preserved for the blanket modules, the divertor components, the inner coils with their supports and the cooling system. The maximum size inside the VV is about 8160 mm in the horizontal direction, and 15 820.5 mm in the vertical direction. Further analysis on gravity load, analysis on frequency and the mode of vibration, and analysis on seismic load are undergoing.

3.3. Divertor

The divertor targets are divided into two halves on each module, as shown in figure 11. The cooling water first inlets to the outer target, then to the inner target, and then to baffles. The cassette is cooled separately, which offers the possibility for the target/baffle maintenance separately, as well as the cassettes segmentation. There are a total of 72 divertor modules, each of them has the weight of ~11 tons. Lower ports for the whole divertor module maintenance require a larger space, while targets and baffles are maintained from upper ports by multi-purpose deployer (MPD), one option of remote handling.

3.4. Tritium breeding blanket

The viability of the deuterium–tritium (DT) fusion as an energy source requires the 'tritium breeding', which is defined as a primary element of the fuel cycle within a fusion reactor, to achieve tritium self-sufficiency. As specified in the CFETR mission, the tritium breading is the one of the top issues, and the CFETR will be operated in the tritium breeding self-sufficiency way. To be able to meet the requirement, the tritium breeding blankets covering almost all the wall of vacuum chamber are necessary. With those blankets, the tritium can be produced and extracted at a rate equal to or slightly larger than tritium consumption in the plasma plus losses caused by radioactive decay from tritium inventories in reactor components. In addition, the tritium breeding blanket also has other functions like heat removal for electricity generation and a shielding capability to protect the superconductor magnet.

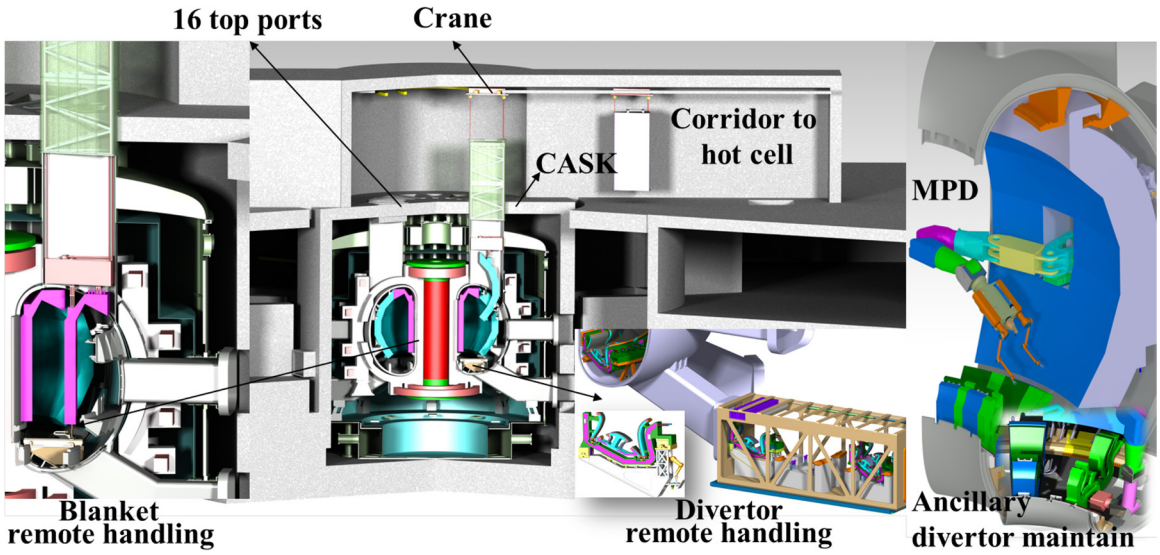

Figure 12. Conceptual design of the CFETR remote handling system.

Based on neutron wall loading, the radial building of each blanket module surrounding the plasma by a series of interaction analyses has been done, as the details given in [18, 19]. Hereafter the structural schemes of the desirable blanket modules can be designed. At present, there are two options of tritium breeding blankets under considerations: one is a helium gas-cooled ceramic breeder blanket (HCCB), the other is a water-cooled ceramic breeder blanket (WCCB). In both options, HCCB is the prime candidate for the CFETR blanket configuration. The engineering design of HCCB is completed. With the specified CFETR blanket configuration, the evaluation of the neutron energy deposition and neutron wall load for the CFETR 1 GW and 2 GW operation is undergoing. Apart from the HCCB design, the design of WCCB is undergoing.

3.5. Remote handling and maintenance system

The burning plasma operation will generate 14 MeV neutrons, which can activate the in-vessel components and materials of CFETR. In addition, the plasma interactions with the stainless steel, tungsten, and graphite tiles used to construct in-vessel components are also expected to generate dust through sputtering, melting, arcing, etc. This dust is both activated and contaminated with tritium that cannot be carried out by operators directly. In this sense, an extensive remote handling and remote maintenance capability within the CFETR facility is extremely needed. However, the remote handling and maintenance (RHM) system design will in turn have a significant impact on the layout of the CFETR and its components/systems designs [20]. As noted by the conservative estimation from CFETR neutronics analysis, the irradiation dose rate within the vacuum vessel during the nuclear phase of operations will be in the range of hundreds of Sv · hr-1 and thus all in-vessel maintenance must be performed by robotic systems. In particular, two primary types of the in-vessel components, tritium breeding blanket and divertor, have to be remote maintained/replaced regularly to meet the requirements of steady-state operation and duty cycle time (30%–50%). [21]. However, the mass and volume of the CFETR tritium breeding blanket and divertor will place a heavier burden on the RHM system, therefore the design of a tritium breeding blanket and divertor should take the capability of the CFETR RHM into account. The design of the CFETR RHM should endow the system with various functions with respect to its handling and maintenance tasks. At present, the engineering analysis on capability of the RHM for in-vessel components has been completed; the strategy of the CFETR RHM system is put forward as shown in figure 12. The tokamak configuration with 16 TF coils and 16 vertical maintenance ports for an inboard and outboard blanket replaced from for high efficiency are considered in this strategy. A permanent corridor with a crane system is used to lift out and transfer the blanket to the hot cell. The divertor will be maintained through four lower ports by the multifunctional platform and transfer cask system in parallel. The multi-purpose deployer (MPD) system will be used to handle ancillary maintenance of blanket and divertor removal and maintain other functions such as dust and tritium inventory control, VV in-service inspection, leak localization, diagnostic maintenance and failure rescue, etc. Safety, reliability, availability and compatibility have been considered during the design process. Within the development of engineering design, the maturity of RHM will grow exponentially in the next step.

4. Summary

As indicated on the roadmap of Chinese magnetic fusion energy development, the CFETR concept design has been carried out for quite a few years. In the last year, a new design with R = 7.2 m and a = 2.2 m for CFETR is proposed with emphasis on high B_T option. Progress on both physics and engineering design is overviewed in this paper.

Recently, the self-consistent steady-state scenario for CFETR with fully sustained non-inductive current drive and as well hybrid mode scenario are developed using a multi-dimensional code suite with physics-based models. The performance

of the two scenarios predicted by the code suite agrees with the estimation by the 0D system code. A fully non-inductive reverse-shear scenario scaled to $R = 7.2$ m, $a = 2.2$ m, $\beta_N \sim 2.4$, $H_{ITER98Y2} \sim 1.25$ and $f_{BS} \sim 0.59$ that meets the CFETR mission with the fusion power production of 1 GW is presented. The scenario presents the solution for the CFETR transport, equilibrium and pedestal dynamics. Some significant contributions of the predicted performance made by the integrated modelling are as follows. (1) The solution illustrates the compatibility of the core performance with the EPED H-mode model and a radiative/detached divertor. (2) Careful examination with the plasma stability indicates that the proposed scenario has a broad operation range in β_N and β_p, which is stable with wall at $r/a = 1.2$. (3) The acceptable core radiation attributed by impurities sets the limit to Z_{eff} of no larger than ~3.0. (4) To meet the minimum fusion power set by the CFETR mission, the helium dilution f_{He} cannot exceed 0.2. (5) To keep the plasma staying in H mode, the tungsten concentration at the edge cannot exceed 3×10^{-5}. The main tasks we needed to tackle in the near-term are to design puff-and-pump radiative divertor compatible with high performance core plasma, to demonstrate compatibility with the alpha particle stability and transport, and to quantify the tritium burn-up rate during the steady-state burning plasma phase in order to find a solution to meet the central fuelling requirement. In addition, the hybrid mode operating scenario that meets the CFETR mission with the fusion power production of 1 GW with R = 7.2 m, a = 2.2 m, $\beta_N \sim 2$, $H_{ITER98Y2} \sim 1.06$ and $f_{BS} \sim 0.50$ that meets the CFETR mission with the fusion power production of 1 GW is also obtained and presented.

And for the integrated engineering design their being conducted, some systems have completed its concept design and continued with the detailed consideration of layout and strategy of the system. However, there are still some critical issues that need to be resolved, including vertical instability control with internal coils, impurity control, alpha particle transport, disruption avoidance and mitigation, type-I ELM control and avoidance, technologies for the large heating power, tritium breeding and handling. More R&D activities are required to resolve those critical issues.

Acknowledgments

This work is supported by the National Magnetic Confinement Fusion Program of China under contract No. 2017YFE0300500 and is supported by the International Partnership Program of the Chinese Academy of Sciences No. Y16YZ17271.

References

[1] Wan Y.X. *et al* 2017 Overview of the present progress and activities on the CFETR *Nucl. Fusion* **57** 102009
[2] Stambaugh R. *et al* 2011 Fusion nuclear science facility candidates *Fusion Sci. Technol.* **59** 279–307
[3] Wan B. *et al* 2014 Physics design of CFETR: determination of the device engineering parameters *IEEE Trans. Plasma Sci.* **42** 495–502
[4] Chan V. *et al* 2015 Evaluation of CFETR as a Fusion Nuclear Science Facility using multiple system codes *Nucl. Fusion* **55** 023017
[5] Shi N. *et al* 2016 Evaluation of CFETR key parameters with different scenarios using system analysis code *Fusion Eng. Des.* **112** 47–52
[6] Meneghini O. *et al* 2016 Integrated fusion simulation with self-consistent core-pedestal coupling *Phys. Plasmas* **23** 042507
[7] Liu L. *et al* 2018 The time-dependent simulation of CFETR baseline steady state scenarios *Nucl. Fusion* **58** 096009
[8] Jian X. *et al* 2018 Application of an empirical saturation rule to TGLF to unity low-*k* and high-*k* turbulence dominated regimes *Nucl. Fusion* **58** 016011
[9] Jian X. *et al* 2017 Optimization of CFETR baseline performance by controlling rotation shear and pedestal collisionality through integrated modelling *Nucl. Fusion* **57** 046012
[10] Chen J. *et al* 2017 Self-consistent modelling of CFETR baseline scenarios for steady state operation *Plasma Phys. Control. Fusion* **59** 075005
[11] Loarte A. *et al* 2007 Progress in the ITER Physics Basis, Chapter 4: power and particle control *Nucl. Fusion* **47** s203–63
[12] Post D. *et al* 1995 A review of recent developments in atomic processes for divertors and edge plasmas *J. Nucl. Mater.* **220–2** 143
[13] Guo H. *et al* 2017 Small angle slot divertor concept for long pulse advanced tokamaks *Nucl. Fusion* **57** 044001
[14] Shi S. *et al* 2018 Evaluating the effects of tungsten on CFETR phase I performance *Nucl. Fusion* **58** 126020
[15] Shi N. *et al* 2017 Study of impurity effects on CFETR steady-state scenario by self-consistent integrated modelling *Nucl. Fusion* **57** 126046
[16] Li Z. *et al* 2018 Ideal MHD stability and characteristics of edge localized modes on CFETR *Nucl. Fusion* **58** 016018
[17] Hou Y.W. *et al* 2018 Analysis of energetic particle driven toroidal Alfven eigenmodes in CFETR baseline scenario *Preprint: 2018 IAEA Fusion Energy Conf. (Gandhinagar, India, 22–27 October 2018)* TH/P2-7
[18] Li J. *et al* 2016 Nuclear-thermal-coupled optimization code for the fusion breeding blanket conceptual design *Fusion Eng. Des.* **113** 37–42
[19] Li J. *et al* 2018 Present state of Chinese magnetic fusion development and future plans *J. Fusion Energy* **38** 113–24
[20] Endrenyi J. *et al* 2007 The present status of maintenance strategies and the impact of maintenance on reliability *IEEE Power Eng. Rev.* **21** 68
[21] Song Y. *et al* 2014 Concept design on RH maintenance of CFETR tokamak reactor *Fusion Eng. Des.* **89** 2331–5
[22] Jardin S.C., Pomphrey N. and Delucia J.L. 1986 Dynamic modeling of transport and positional control of tokamaks *J. Comput. Phys.* **66** 481
[23] Humphreys D.A. *et al* 2007 Development of ITER-relevant plasma control solutions at DIII-D *Nucl. Fusion* **47** 943
[24] Chan V.S. *et al* 2010 Physics basis of a fusion development facility utilizing the tokamak approach *Fusion Sci. Technol.* **57** 66–93
[25] Cheng S.-K. *et al* 2019 Dominant two-fluid MHD instabilities in CFETR upgrade phase-I scenario in presence of perfect conducting wall *Plasma Phys. Control. Fusion* **61** 045009
[26] Garofalo A.M. *et al* 2015 The quiescent H-mode regime for high performance edge localized mode-stable operation in future burning plasmas *Phys. Plasmas* **22** 056116
[27] Meneghini O. *et al* 2013 Integrated modeling of tokamak experiments with OMFIT *Plasma Fusion Res.* **8** 2403009
[28] Meneghini O. *et al* 2015 Integrated modeling applications for tokamak experiments with OMFIT *Nucl. Fusion* **55** 083008

[29] Candy J. *et al* 2009 Tokamak profile prediction using direct gyrokinetic and neoclassical simulation *Phys. Plasmas* **16** 060704
[30] Staebler G.M. *et al* 2005 Gyro-Landau fluid equations for trapped and passing particles *Phys. Plasmas* **12** 102508
[31] Staebler G.M. *et al* 2007 A theory-based transport model with comprehensive physics *Phys. Plasmas* **14** 055909
[32] Belli E.A. *et al* 2008 Kinetic calculation of neoclassical transport including self-consistent electron and impurity dynamics *Plasma Phys. Control. Fusion* **50** 095010
[33] Snyder P.B. *et al* 2009 Development and validation of a predictive model for the pedestal height *Phys. Plasmas* **16** 056118
[34] Pfeiffer W.W. *et al* 1980 ONETWO: a computer code for modeling plasma transport in tokamaks *General Atomics Report* GA-A16178 (San Diego, CA: General Atomic Co.)
[35] Lin-Liu Y.R. *et al* 2003 Electron cyclotron current drive efficiency in general tokamak geometry *Phys. Plasmas* **10** 4064–71
[36] Wright J.C. *et al* 2010 Challenges in self-consistent full-wave simulations of lower hybrid waves *IEEE Trans. Plasma Sci.* **38** 2136–43
[37] Brambilla M. 1999 Numerical simulation of ion cyclotron waves in tokamak plasmas *Plasma Phys. Control. Fusion* **41** 1
[38] Pankin A. *et al* 2004 The tokamak Monte Carlo fast ion module NUBEAM in the National Transport Code Collaboration library *Comput. Phys. Commun.* **159** 157–84
[39] Lao L.L. *et al* 1985 Reconstruction of current profile parameters and plasma shapes in tokamaks *Nucl. Fusion* **25** 1611
[40] Lao L.L. *et al* 2005 MHD equilibrium reconstruction in the DIII-D tokamak *Fusion Sci. Technol.* **48** 968–77
[41] Artaud J.F. *et al* 2008 METIS user's guide *Technical Report* CEA, IRFM
[42] Artaud J.F. *et al* 2010 The CRONOS suite of codes for integrated tokamak modelling *Nucl. Fusion* **50** 043001
[43] Crotinger J.A. *et al* 1997 *LLNL Report* UCRL ID-126284, NTIS #PB2005-102154
[44] Schneider R. *et al* 2006 Plasma edge physics with B2-Eirene *Contrib. Plasma Phys.* **46** 3–191
[45] Cheng C.Z. 1992 Kinetic extensions of magnetohydrodynamics for axisymmetric toroidal plasmas *Phys. Rep.* **211** 1–51
[46] Sovinec C.R. *et al* 2004 Nonlinear magnetohydrodynamics simulation using high-order finite elements *J. Comput. Phys.* **195** 355–86
[47] Hou Y. *et al* 2018 NIMROD calculations of energetic particle driven toroidal Alfvén eigenmodes *Phys. Plasmas* **25** 012501
[48] Zheng J.X. *et al* 2019 Electromagnetic design and challenges for 14 T high-Tc toroidal field superconducting magnet for CFETR *IEEE Trans. Appl. Supercond.* **29** 4600104